

ESI material for the manuscript:

Polymorphism of oxindole as the core structure in bioactive compounds

Barbara Hachuła,^{*a} Maciej Zubko,^b Paweł Zajdel,^c Maria Książek,^c Joachim Kusz,^c
Oliwia Starczewska,^b Joanna Janek^a and Wojciech Pisarski^a

^a Institute of Chemistry, University of Silesia, Szkolna 9, 40-006 Katowice, Poland

^b Institute of Materials Science, University of Silesia, 75 Pułku Piechoty 1a,
41-500 Chorzów, Poland

^c Institute of Physics, University of Silesia, Uniwersytecka 4, 40-007 Katowice, Poland

Table of Contents

- SI 1. Crystal Growth and Polymorph Identification
- SI 2. Single Crystal X-ray Diffraction
- SI 3 Crystal structure analysis
- SI 4 Powder X-ray Diffraction (PXRD)
- SI 5. Hirshfeld Surface Analysis
- SI 6. Infrared Spectroscopy
- SI 7. Differential Scanning Calorimetry (DSC)

SI 1. Crystal growth and polymorph identification

Crystallization experiments carried out from the commercial substance at RT (Sigma-Aldrich 97 %) in several solvents: water, acetone, methanol, ethanol, 2-propanol, chloroform, ethyl acetate, toluene, resulted in the formation of four polymorphic forms. Three of the polymorphs (α -, β - and γ -forms) could be obtained selectively by evaporation of a solution of the compound from different solvents whereas the crystals of δ -form grow only once as needles in ethanol (Figure S1, Table S1).

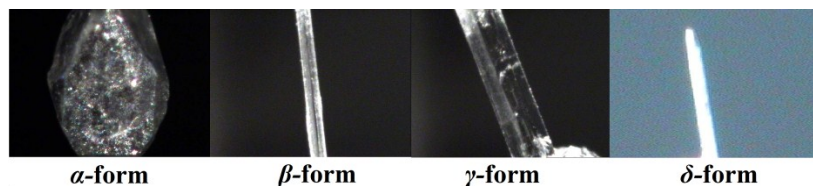


Figure S1. Optical micrographs of (a) polyhedron, (b) needle, (c) plate (d) needle, crystals of OX polymorphs used for crystal structure determination.

Table S1. Results of crystallization experiments on oxindole system

Photograph	Polymorphic form	Growth conditions
	α -form (polyhedron)	Crystallization of the commercial substance from a 1:1 mixture of acetone and water at RT
	β -form (needles)	Crystallization of the commercial substance from acetone, methanol, ethanol, 2-propanol, ethyl acetate, toluene at RT and crystallization from the melt
	γ -form (plates)	Crystallization of the commercial substance from chloroform at RT

SI 2. Single-crystal X-ray diffraction (XRD)

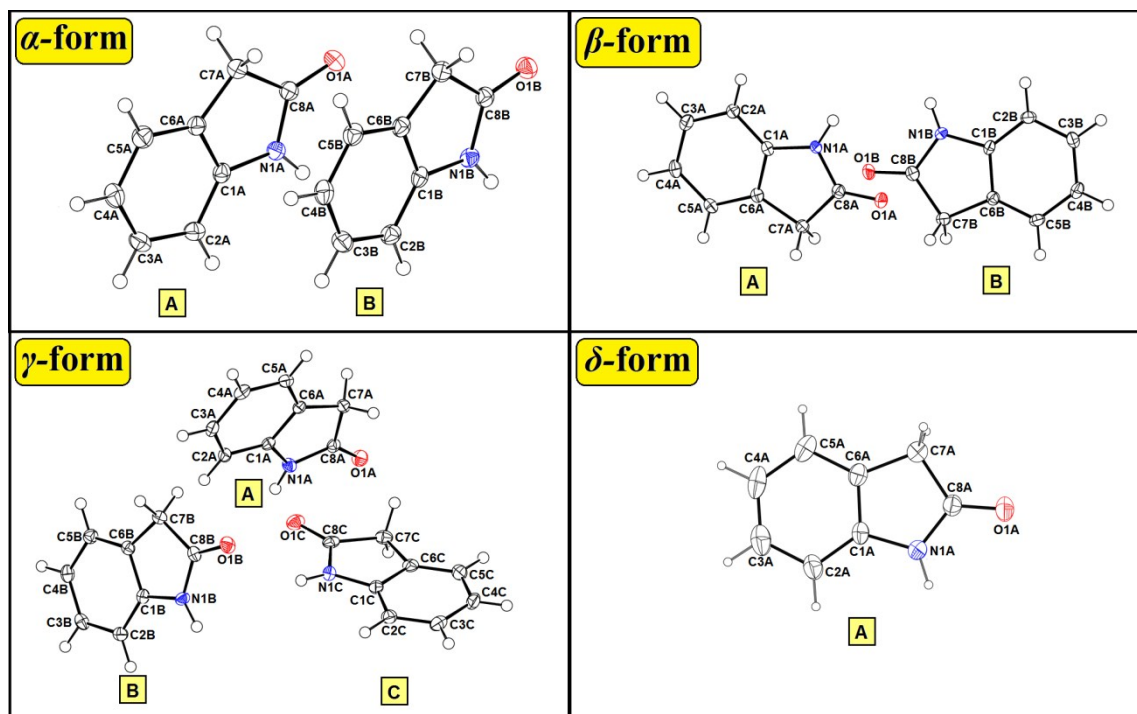


Figure S2. ORTEP of four polymorphic forms of OX with 50 % probability ellipsoids.

Table S2. Crystallographic data for four polymorphic forms of OX at 293 K and 100 K

	α -form		β -form		γ -form		δ -form	
Chemical formula	C ₈ H ₇ NO		C ₈ H ₇ NO		C ₈ H ₇ NO		C ₈ H ₇ NO	
Compound weight	133.15		133.15		133.15		133.15	
Crystal system	Monoclinic		Monoclinic		Triclinic		Monoclinic	
Space group	<i>P</i> 2 ₁ /c		<i>P</i> 2 ₁ /c		<i>P</i> 1̄		<i>P</i> 2 ₁ /c	
Crystal dimension (mm ³)	0.38 × 0.36 × 0.36		0.60 × 0.08 × 0.04		0.60 × 0.17 × 0.09		0.20 × 0.03 × 0.02	
Crystal form	Polyhedron		Needle		Plate		Needle	
<i>T</i> / K	293	100	293	100	293	100	293	100
<i>a</i> / Å	12.7471(5)	12.8234(3)	14.4305(9)	14.2644(9)	5.6520(5)	5.6075(1)	12.2387(7)	12.0455(3)
<i>b</i> / Å	8.2941(3)	8.0674(2)	13.1657(10)	12.9569(8)	13.1283(18)	13.0331(3)	7.2236(4)	7.0949(2)
<i>c</i> / Å	13.5772(6)	13.4505(3)	7.0872(5)	6.9931(4)	14.9297(10)	14.8275(3)	8.0822(4)	7.9670(2)
α / °	90	90	90	90	114.314(19)	114.825(2)	90	90
β / °	111.406(5)	111.531(2)	101.958(7)	100.393(6)	100.619(10)	100.483(2)	103.325(6)	101.314(3)
γ / °	90	90	90	90	91.595(9)	91.664(2)	90	90
<i>V</i> / Å ³	1336.44(9)	1294.38(5)	1317.26(16)	1271.28(13)	985.6(2)	960.32(3)	695.29(7)	667.64(3)
<i>Z</i>	8	8	8	8	6	6	4	4
<i>D</i> _{calc} / cm ⁻³	1.323	1.366	1.343	1.391	1.346	1.381	1.275	1.325
<i>F</i> (000)	560	560	560	560	420	420	280	280
Reflns collected	8578	8307	8745	8282	6889	7481	5463	5323
Reflns independent	2359	2296	2327	2253	3423	3329	1417	1366
<i>R</i> ₁ values (<i>I</i> > 2σ(<i>I</i>))	0.0316	0.0288	0.0467	0.0348	0.0303	0.0290	0.0499	0.0353
<i>wR</i> (<i>F</i> ²) values (<i>I</i> > 2σ(<i>I</i>))	0.0585	0.0806	0.0774	0.0615	0.0749	0.0896	0.1220	0.0956
<i>R</i> ₁ values (all data)	0.0538	0.0354	0.1045	0.0712	0.0437	0.0344	0.0809	0.0422
<i>wR</i> (<i>F</i> ²) values (all data)	0.0607	0.0828	0.0839	0.0651	0.0779	0.0917	0.1518	0.1024
CCDC deposition no.	817385	817386	817387	817388	817389	817390	1526388	1526389

SI 3. Crystal structure analysis

Table S3. Selected bond lengths (\AA) and angles ($^{\circ}$) for the four forms of oxindole at 100K

	α -form	β -form	γ -form	δ -form	Mean value
O1—C8	1.2317(14) (A)	1.233(2) (A)	1.2224(14) (A)	1.2294(14)	1.2311
	1.2355(14) (B)	1.234(2) (B)	1.2319(14) (B)		
			1.2311(15) (C)		
N1—C8	1.3540(15) (A)	1.363(2) (A)	1.3636(15) (A)	1.3540(15)	1.3587
	1.3549(14) (B)	1.360(2) (B)	1.3582(15) (B)		
			1.3618(15) (C)		
N1—C1	1.4030(14) (A)	1.403(2) (A)	1.4048(15) (A)	1.4004(14)	1.4057
	1.4078(15) (B)	1.410(2) (B)	1.4087(15) (B)		
			1.4080(15) (C)		
C1—C2	1.3836(15) (A)	1.385(2) (A)	1.3813(16) (A)	1.3785(17)	1.3817
	1.3776(16) (B)	1.377(2) (B)	1.3847(16) (B)		
			1.3857(16) (C)		
C1—C6	1.3936(16) (A)	1.392(2) (A)	1.3997(16) (A)	1.4006(17)	1.3965
	1.3975(15) (B)	1.389(2) (B)	1.4019(16) (B)		
			1.3975(16) (C)		
C2—C3	1.3927(16) (A)	1.393(2) (A)	1.3952(17) (A)	1.3928(18)	1.3933
	1.3910(17) (B)	1.396(2) (B)	1.3950(17) (B)		
			1.3907(18) (C)		
C3—C4	1.3850(17) (A)	1.385(2) (A)	1.3881(17) (A)	1.389(2)	1.3870
	1.3883(18) (B)	1.383(2) (B)	1.3890(18) (B)		
			1.3887(17) (C)		
C4—C5	1.3959(16) (A)	1.400(3) (A)	1.3939(17) (A)	1.3955(18)	1.3948
	1.3937(17) (B)	1.395(3) (B)	1.3919(17) (B)		
			1.3926(18) (C)		

C5—C6	1.3798(16) (A) 1.3808(16) (B)	1.384(2) (A) 1.380(3) (B)	1.3862(16) (A) 1.3795(16) (B) 1.3819(17) (C)	1.3815(16)	1.3817
C6—C7	1.5039(15) (A) 1.5001(16) (B)	1.504(2) (A) 1.514(3) (B)	1.5049(16) (A) 1.5021(16) (B) 1.5006(17) (C)	1.5023(16)	1.504
C7—C8	1.5210(17) (A) 1.5123(16) (B)	1.519(2) (A) 1.520(2) (B)	1.5189(16) (A) 1.5131(17) (B) 1.5218(18) (C)	1.5214(16)	1.5184
C8—N1—C1	111.82(10) (A) 111.71(10) (B)	111.47(16) (A) 111.55(15) (B)	111.91(10) (A) 111.49(10) (B) 111.61(10) (C)	112.00(9)	111.69
C2—C1—N1	128.27(11) (A) 129.05(10) (B)	127.84(17) (A) 128.01(17) (B)	128.11(10) (A) 128.63(11) (B) 128.49(11) (C)	128.32(11)	128.34
C6—C1—N1	109.39(10) (A) 108.80(10) (B)	109.50(16) (A) 109.62(16) (B)	109.29(10) (A) 109.23(10) (B) 109.10(10) (C)	108.97(10)	109.24
O1—C8—N1	125.07(11) (A) 125.62(11) (B)	125.26(18) (A) 125.24(17) (B)	125.40(11) (A) 125.66(11) (B) 125.18(11) (C)	123.92(11)	125.17
O1—C8—C7	127.21(10) (A) 126.31(10) (B)	126.91(17) (A) 126.91(17) (B)	127.20(10) (A) 126.33(11) (B) 127.23(11) (C)	128.11(10)	127.03
N1—C8—C7	107.72(9) (A) 108.07(10) (B)	107.83(16) (A) 107.85(16) (B)	107.40(10) (A) 108.01(10) (B) 107.58(10) (C)	107.97(9)	107.80

Table S4. Characteristics of hydrogen-bond geometries observed in the crystal structures of four forms of OX at 295 K.

$D\text{---H}\cdots A$ (symmetry code)	$D\text{---H}$ (Å)	$H\cdots A$ (Å)	$D\cdots A$ (Å)	$D\text{---H}\cdots A$ (deg)
α -form				
N1—H1N···O1A (1-x,2-y,2-z)	0.879(15)	1.940(15)	2.8169(15)	175.5(13)
O1···H1NA—N1A (1-x,2-y,2-z)	0.885(14)	2.140(14)	3.0088(15)	167.1(12)
O1···H7AA—C7A (1-x,1/2+y,2.5-z)	0.957(14)	2.424(14)	3.3386(17)	159.9(11)
C5A—H5A···O1A (1-x,-1/2+y,2.5-z)	0.947(15)	2.641(16)	3.5878(19)	177.8(12)
O1···H7BA—C7A(x,y,x)	1.001(14)	2.673(14)	3.2629(19)	117.8(9)
C4—H4···O1A (-1+x,1.5-y,-1/2+z)	0.979(16)	2.719(16)	3.4346(19)	130.4(11)
C3—H3···O1A (-1+x,1.5-y,-1/2+z)	0.959(14)	2.928(14)	3.5216(18)	121.2(10)
C3—H3···N1 (-x,-1/2+y,1.5-z)	0.959(14)	3.020(15)	3.8491(19)	145.6(11)
β -form				
O1···H1NA—N1A (x,1/2-y,1/2+z)	0.88(2)	1.97(2)	2.842(2)	170(2)
N1—H1N···O1A (x,1/2-y,1/2+z)	0.94(2)	1.93(2)	2.865(2)	171(2)
O1···H5A—C5A (1-x,1-y,2-z)	0.99(2)	2.59(2)	3.307(3)	129.1(17)
C5—H5···O1A (-x,1-y,1-z)	0.97(2)	2.60(2)	3.338(3)	132.7(17)
O1···H7BA—C7A (x,y,z)	0.95(2)	2.72(2)	3.345(3)	124.2(18)
C7—H7B···O1A (x,y,z)	0.99(2)	2.80(2)	3.325(3)	114.2(15)
O1···H4A—C4A (1-x,1-y,2-z)	1.00(2)	2.78(2)	3.402(3)	121.3(16)
C4—H4···O1A (-x,1-y,1-z)	0.99(2)	2.86(2)	3.502(3)	123.7(17)
N1—H1N···N1A (x,1/2-y,1/2+z)	0.94(2)	2.96(2)	3.584(3)	124.9(16)
N1···H1NA—N1A (x,1/2-y,1/2+z)	0.88(2)	3.00(2)	3.584(3)	125.5(18)
γ -form				
N1—H1N···O1A (x,y,z)	0.853(12)	2.081(13)	2.8838(13)	156.6(12)
N1A—H1NA···O1B(-1+x,y,z)	0.848(14)	2.154(14)	2.9467(15)	155.6(12)
O1···H1NB—N1B (1+x,y,z)	0.902(14)	2.333(13)	3.0700(15)	138.9(12)
O1A···H1NB—N1B (x,y,z)	0.902(14)	2.376(14)	3.1161(16)	139.4(11)
O1···H2B—C2B (1+x,y,z)	0.947(14)	2.533(14)	3.2723(18)	135.1(11)
O1···H7BB—C7B (x,y,z)	0.990(14)	2.635(14)	3.0739(19)	107.0(10)
C7—H7B···O1A (1+x,y,z)	0.926(12)	2.671(12)	3.2420(16)	120.6(9)
O1B···H7AB—C7B (1-x,2-y,1-z)	0.969(15)	2.765(14)	3.4608(19)	129.3(10)
C2—H2···O1A (x,y,z)	0.964(12)	2.824(13)	3.4998(18)	127.9(9)
C2A—H2A···O1B (-1+x,y,z)	0.924(14)	2.835(13)	3.5044(18)	130.3(10)
O1···H1NA—N1A (1+x,y,z)	0.848(14)	2.953(13)	3.5164(15)	125.8(10)
N1B···H7BB—C7B (-1+x,y,z)	0.990(14)	3.052(14)	4.0335(18)	171.3(11)
δ -form				
N1A—H1A···O1A (1-x, 1/2+y,1.5-z)	0.91(2)	1.87(2)	2.782(2)	173.8(18)
C7A—H7A···O1A (1-x,-y,1-z)	0.97(2)	2.92(2)	3.857(3)	163.5(16)
C7A—H7A···O1A (x, 1/2-y,- 1/2+z)	0.97(2)	2.90(2)	3.466(3)	118.5(14)
C7A—H7A···N1A (x, 1/2-y,-1/2+z)	0.97(2)	2.933(19)	3.673(2)	134.3(14)

Table S5. Characteristics of hydrogen-bond geometries observed in crystal structures of four forms of OX at 100 K.

D—H···A (symmetry code)	D—H (Å)	H···A (Å)	D···A (Å)	D—H···A (deg)
α-form				
N1A—H1NA···O1B (1-x,2-y,2-z)	0.875(14)	1.923(14)	2.7974(13)	176.9(12)
O1A···H1NB—N1B (1-x,2-y,2-z)	0.887(14)	2.105(14)	2.9793(13)	168.5(11)
O1A···H7AB—C7B (1-x, $\frac{1}{2}$ +y,2.5-z)	0.989(13)	2.335(13)	3.2892(14)	161.8(10)
C5B—H5B···O1B (1-x,- $\frac{1}{2}$ +y,2.5-z)	0.980(14)	2.556(14)	3.5342(15)	176.6(10)
O1A···H7BB—C7B (x,y,x)	0.972(14)	2.636(13)	3.2149(15)	118.4(9)
C4A—H4A···O1B (-1+x,1.5-y,- $\frac{1}{2}$ +z)	0.936(14)	2.681(14)	3.5338(15)	129.4(10)
C3A—H3A···O1B (-1+x,1.5-y,- $\frac{1}{2}$ +z)	0.973(13)	2.827(13)	3.4372(14)	121.5(9)
C3A—H3A···N1A (-x,- $\frac{1}{2}$ +y,1.5-z)	0.973(13)	2.922(13)	3.7611(16)	145.1(10)
β-form				
O1A···H1NB—N1B (x, $\frac{1}{2}$ -y, $\frac{1}{2}$ +z)	0.886(18)	1.956(19)	2.8338(19)	170.7(16)
N1A—H1NA···O1B (x, $\frac{1}{2}$ -y, $\frac{1}{2}$ +z)	0.900(18)	1.967(18)	2.8556(19)	169.0(16)
O1A···H5B—C5B (1-x,1-y,2-z)	0.962(18)	2.550(18)	3.251(2)	129.8(13)
C5A—H5A···O1B (-x,1-y,1-z)	0.947(18)	2.592(17)	3.284(2)	130.2(13)
O1A···H7BB—C7B (x,y,z)	0.964(18)	2.624(18)	3.246(2)	122.6(13)
C7A—H7BA···O1B (x,y,z)	0.991(18)	2.729(17)	3.262(2)	114.2(12)
O1A···H4B—C4B (1-x,1-y,2-z)	0.997(18)	2.741(17)	3.349(2)	119.7(12)
C4A—H4A···O1B (-x,1-y,1-z)	1.024(18)	2.824(17)	3.432(2)	118.5(12)
N1A—H1NA···N1B (x, $\frac{1}{2}$ -y, $\frac{1}{2}$ +z)	0.900(18)	2.979(18)	3.583(2)	126.1(13)
N1A···H1NB—N1B (x, $\frac{1}{2}$ -y, $\frac{1}{2}$ +z)	0.886(18)	2.991(17)	3.583(2)	126.0914
γ-form				
N1A—H1NA···O1B (x,y,z)	0.873(14)	2.043(14)	2.8628(13)	156.0(12)
N1B—H1NB···O1A (-1+x,y,z)	0.877(14)	2.057(14)	2.8925(13)	158.9(12)
O1A···H1NC—N1C (1+x,y,z)	0.909(14)	2.287(13)	3.0189(12)	137.4(11)
O1B···H1NC—N1C (x,y,z)	0.909(14)	2.326(14)	3.0821(13)	140.5(11)
O1A···H2C—C2C (1+x,y,z)	0.956(13)	2.475(14)	3.2174(15)	134.4(10)
O1A···H7BC—C7C (x,y,z)	0.996(14)	2.559(13)	3.0226(15)	108.3(9)
C7A—H7BA···O1B (1+x,y,z)	0.954(13)	2.639(12)	3.2077(14)	118.6(9)
O1C···H7AC—C7C (1-x,2-y,1-z)	0.968(14)	2.695(14)	3.3893(15)	129.0(10)
C2A—H2A···O1B (x,y,z)	0.956(13)	2.819(13)	3.4818(14)	127.2(10)
C2B—H2B···O1C (-1+x,y,z)	0.968(14)	2.879(13)	3.5187(15)	124.5(9)
O1A···H1NB—N1B (1+x,y,z)	0.877(14)	2.980(14)	3.5335(13)	122.9(10)
N1C···H7BC—C7C (-1+x,y,z)	0.996(14)	2.989(14)	3.9789(16)	172.5(10)
δ-form				
N1A—H1A···O1A (1-x, $\frac{1}{2}$ +y,1.5-z)	0.907(15)	1.871(15)	2.7706(13)	171.0(12)
C7A—H7A···O1A (1-x,-y,1-z)	0.982(14)	2.787(15)	3.7353(15)	162.5(11)
C7A—H7A···O1A (x, $\frac{1}{2}$ -y,- $\frac{1}{2}$ +z)	0.982(14)	2.821(14)	3.3859(14)	117.3(10)
C7A—H7A···N1A (x, $\frac{1}{2}$ -y,- $\frac{1}{2}$ +z)	0.982(14)	2.885(14)	3.6007(14)	130.5(10)

Table S6. The first and second level hydrogen bond graph set matrix of four forms of OX

	a	b	c	
α -form	a $D(2)$	—	—	—
	b $R_2^2(8) > a > b$	$D(2)$	—	—
β -form	a $D(2)$	—	—	—
	b $R_2^2(8) > a > b$	$D(2)$	—	—
γ -form	a $D(2)$	—	—	—
	b $D_2^2(6) > a > b$	$D(2)$	—	—
	c $D_2^2(6) > a > c$	$D_2^2(6) > b > c$	$D(2)$	—
	d $D_2^1(3) > a > d$	$C_2^2(8) > b > d$	$D_1^2(3) > c > d$	$D(2)$
δ -form	a $C(4)$	—	—	—

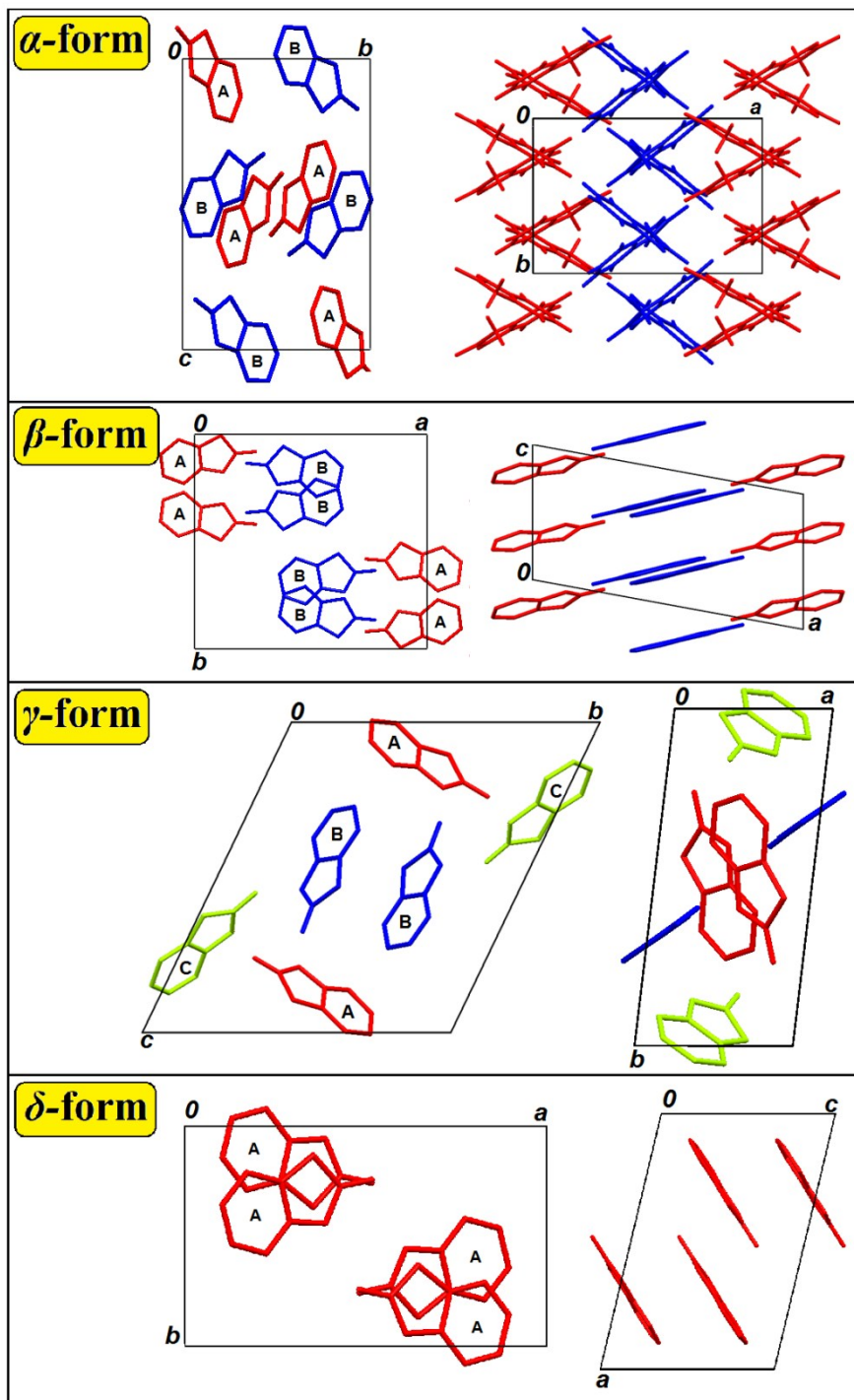


Figure S3. Packing structure of α - and γ -forms observed along (a) the a -axis and (b) the c -axis. Packing structure of β - and δ -forms observed along (a) the c -axis and (b) the b -axis. Molecules have been coloured by symmetry equivalence.

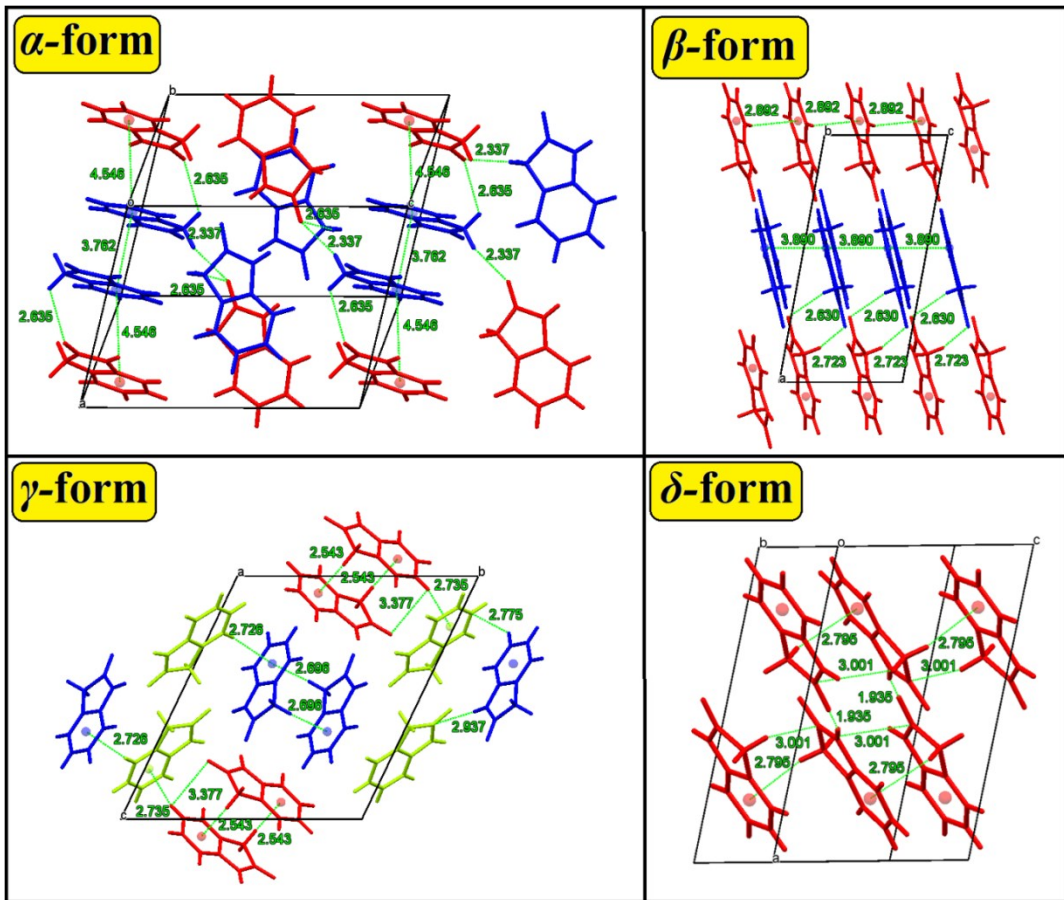


Figure S4. A weak C-H···O, C-H···π and π···π interactions in the crystal lattices of four forms of OX.

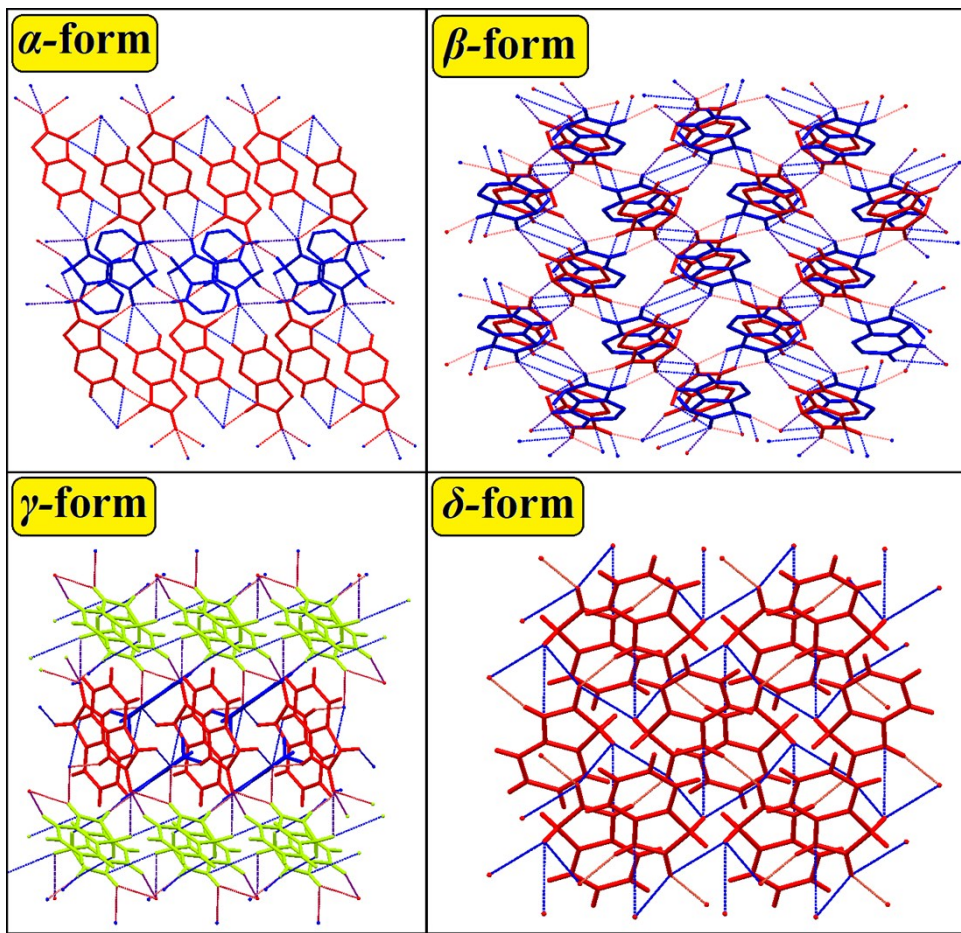


Figure S5. 3D hydrogen-bonded network of α -form (ac plane), β -form (bc plane), γ -form (ab plane) and δ -form (bc plane). Hydrogen bonds are shown as dashed lines.

SI 4 Powder X-ray Diffraction (PXRD)

Powder diffraction studies have been carried out at room temperature on a PANalytical PW1050 diffractometer using nickel filtered Cu $K\alpha_{1,2}$ source operating at 30 kV/30 mA. White, polycrystalline samples were scraped from Petri dishes, ground in an agate mortar and specimens were deposited on a double-sided scotch tape attached to a glass slide. Diffractograms were collected in an angular range $6 - 37^\circ$ with a 0.02° step.

A typical PXRD acquisition in our lab consist of 4 passes over the same angular range, which are later merged into one file. In this case, after the first trials it became evident that the first and the last runs differ therefore subsequent runs were carried out using more runs with acquisitions times from 1s to 12 s per point to cover wider timespan. The collected patters were later separated and each of them was associated with a time, which elapsed from the beginning of the experiment to the middle of the current run. This became later the basis for the x -axis on all plots.

All patterns for each time run were also summed into one dataset, which was later used to calibrate zero shift, displacement and surface roughness corrections for the Rietveld refinement. The Rietveld refinement was carried out using Fullprof Suite from cif files obtained from single crystal diffraction and required only refinement of an isotropic atomic displacement parameter for each phase and scale. During the measurements, we have not observed any changes in the background, which (if present) would suggest an appearance/disappearance of an amorphous component. Therefore we concluded that the phase transformation takes place only between the original phase (β or γ) and the α -form. Assuming that the sum of mass does not change (no contribution from amorphous phases) a simple model of time evolution was suggested, where the mass fraction of one form is transformed into another one with time constant τ :

$$M_{\beta \text{ or } \gamma} + M_{\alpha} = \text{const}$$

$$dM_{\beta \text{ or } \gamma} = - dM_{\alpha}, dM_{\beta \text{ or } \gamma} = -\tau^{-1}_{\beta \text{ or } \gamma \rightarrow \alpha} dt$$

Therefore

$$M_{\beta \text{ or } \gamma} = M_{\beta \text{ or } \gamma}(0) \exp(-t/\tau_{\beta \text{ or } \gamma \rightarrow \alpha}) (*)$$

$$M_{\alpha}(0) = M_{\beta \text{ or } \gamma}(0) (1 - \exp(-t/\tau_{\beta \text{ or } \gamma \rightarrow \alpha}))$$

Equation (*) has been fitted to both decay curves obtained in the experiment. Please note that from the current experiment we are not able to determine the absolute activation energy of each process but only a relative dimensionless value ($\tau_{\gamma \rightarrow \alpha}/\tau_{\beta \rightarrow \alpha}$), which was reported in the paper.

The fits resulted in the following values of refined parameters (all uncertainties are statistical on 1- σ level).

Transformation β to α :

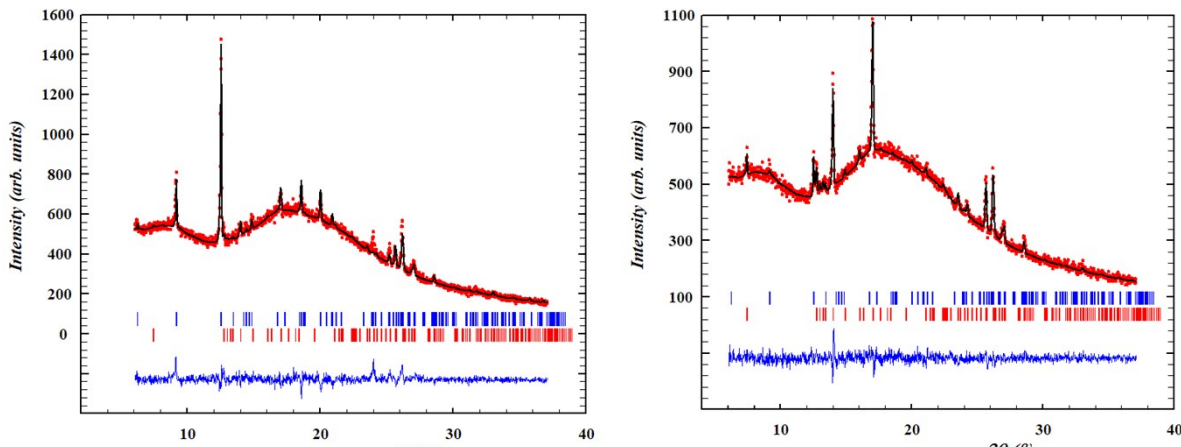
$$\chi^2 = 14, R=0.98, M_{\beta}(0) = 99.5 \pm 3.1, \tau_{\beta \rightarrow \alpha} = 10.9 \pm 0.5$$

The high value of χ^2 is related to only one point, which is separated from the line by more than 1- σ but less than 2- σ .

Transformation γ to α :

$$\chi^2 = 0.3383, R=0.98, M_{\gamma}(0) = 99.8 \pm 0.3, \tau_{\gamma \rightarrow \alpha} = 119 \pm 6$$

Below we present examples of refinements to the first and the last pattern in each series.



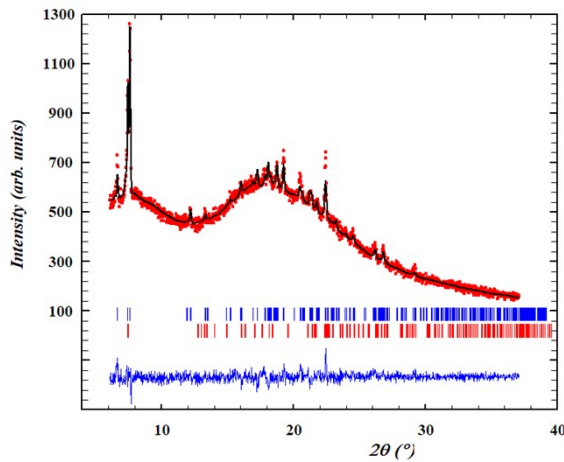


Figure S8. Rietveld refinement of the first pattern of the γ -type PXRD. Upper ticks (blue) γ -type (100(2) %), bottom ticks (red) α -type.

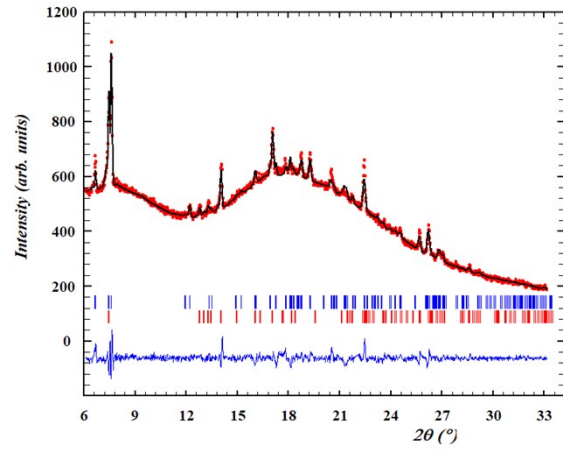


Figure S9. Rietveld refinement of the first pattern of the γ -type PXRD. Upper ticks (blue) γ -type (86(2) %), bottom ticks (red) α -type.

SI 5. Hirshfeld Surface Analysis

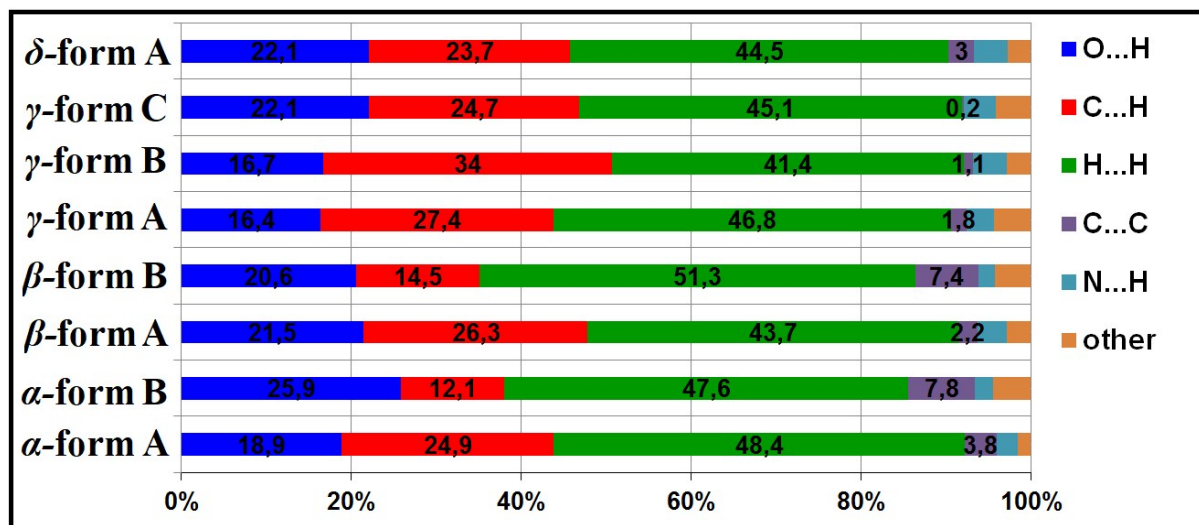


Fig. S10. Percentage contributions to the Hirshfeld surface area for the various close

intermolecular contacts for molecules in the four forms of OX. Percentages are given on the histogram detail in the text.

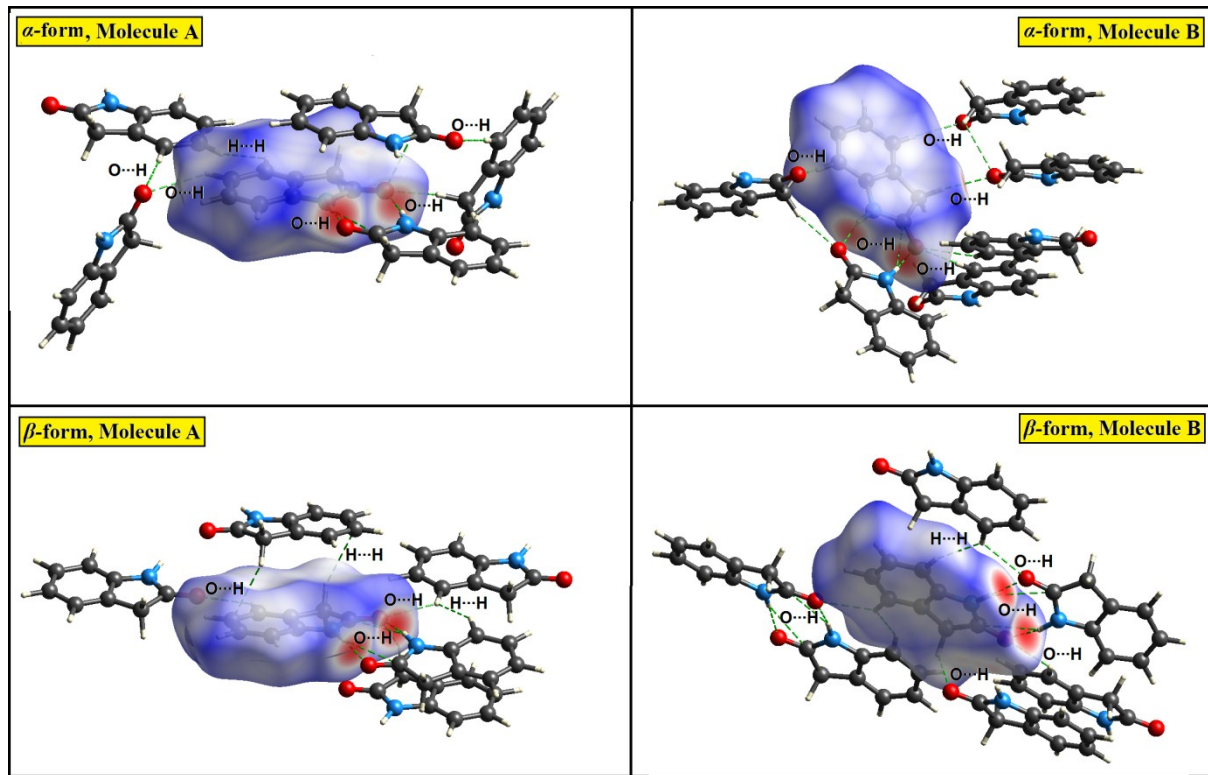


Figure S11. d_{norm} mapped on Hirshfeld surface for visualizing the intermolecular interactions in the molecules of (top) α -form and (bottom) β -form. Dotted lines (green) represent hydrogen bonds.

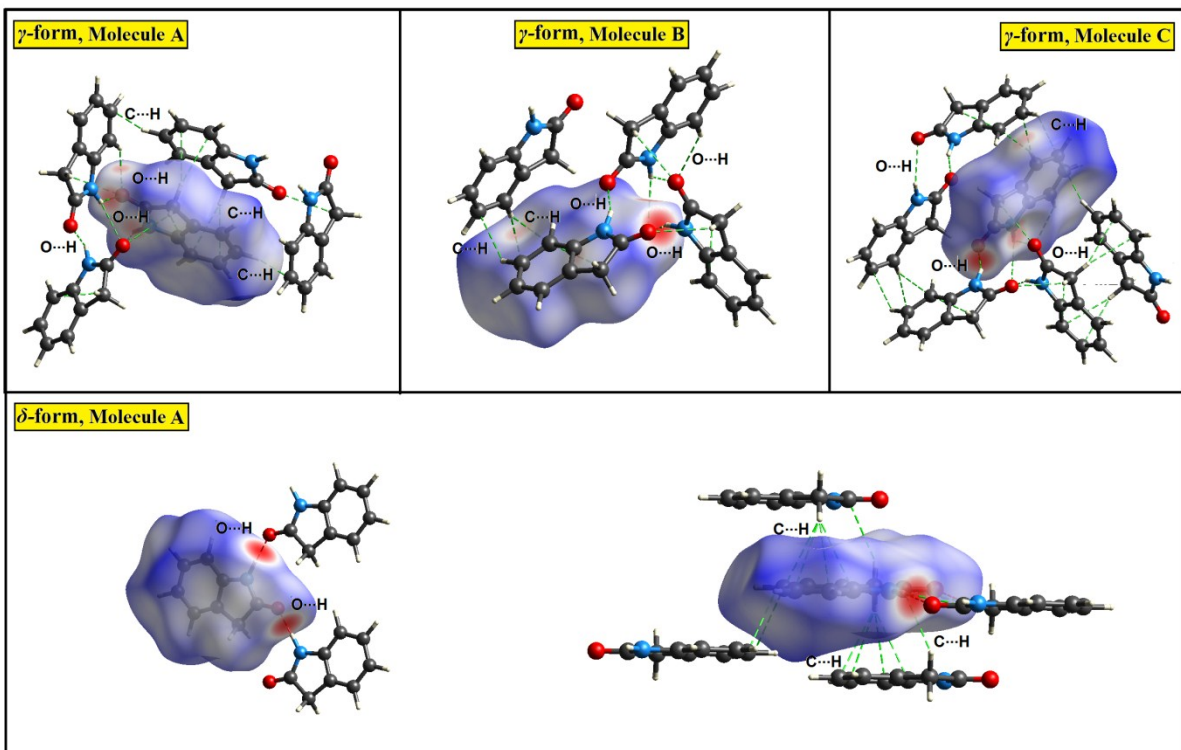


Figure S12. d_{norm} mapped on Hirshfeld surface for visualizing the intermolecular interactions in the molecules of (upper) γ -form and (bottom) δ -form. Dotted lines (green) represent hydrogen bonds

SI 6. Infrared Spectroscopy

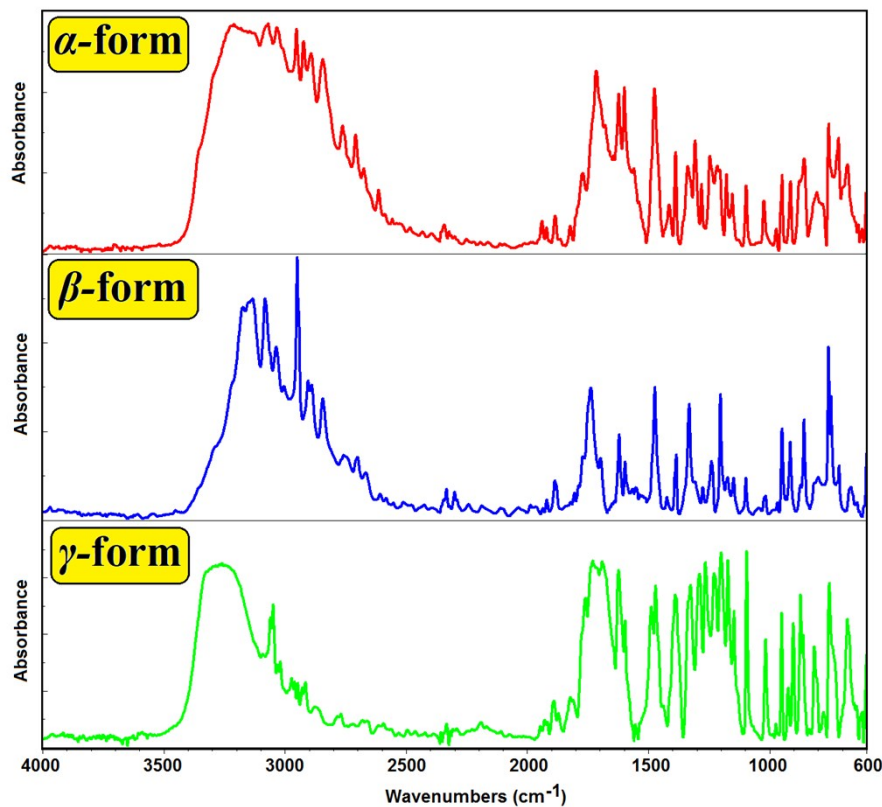


Figure S13. ATR-IR spectra of three polymorphic forms of OX recorded at RT

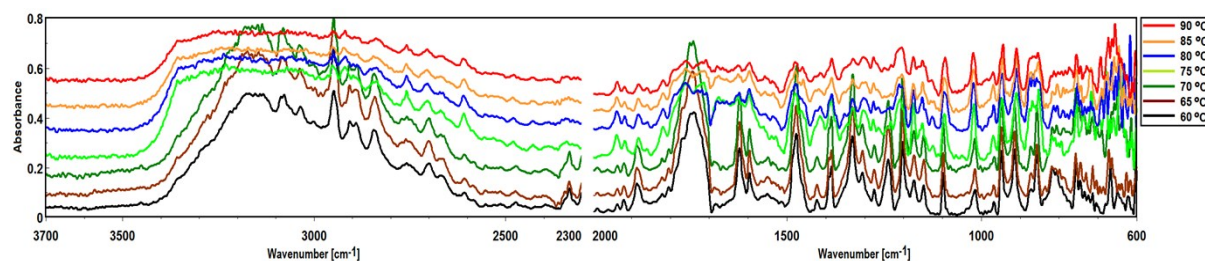


Figure S14. Temperature-dependent IR spectra in the region of (left) 3700-2300 cm⁻¹ and (right) 2000-600 cm⁻¹ collected during the heating process of β-form.

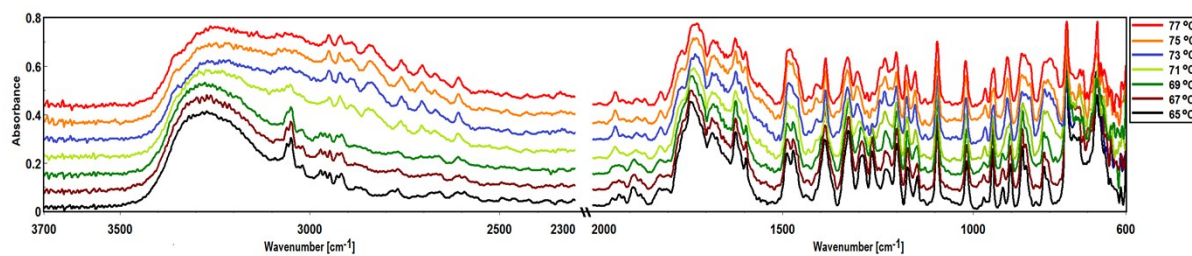


Figure S15. Temperature-dependent IR spectra in the region of (left) 3700-2300 cm⁻¹ and (right) 2000-600 cm⁻¹ collected during the heating process of γ-form.

SI 7. Differential Scanning Calorimetry (DSC)

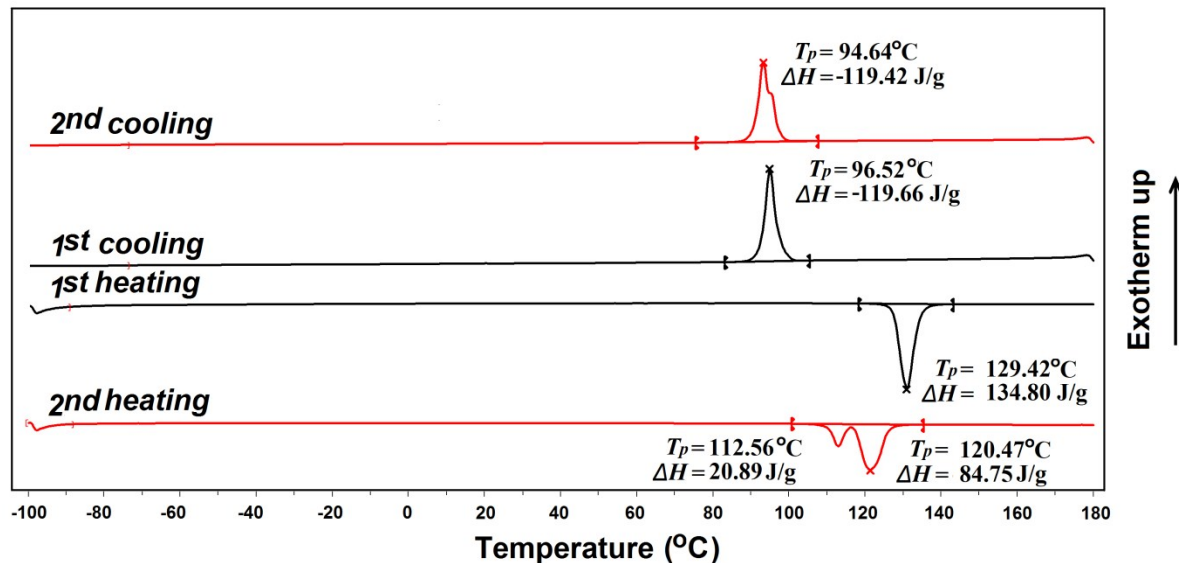


Figure S16. DSC curves of α -form, recorded with a heating and cooling rate of $20^\circ\text{C min}^{-1}$. Peak temperatures (T_p) and the heat of fusion (ΔH) are given in $^\circ\text{C}$ and J g^{-1} , respectively.

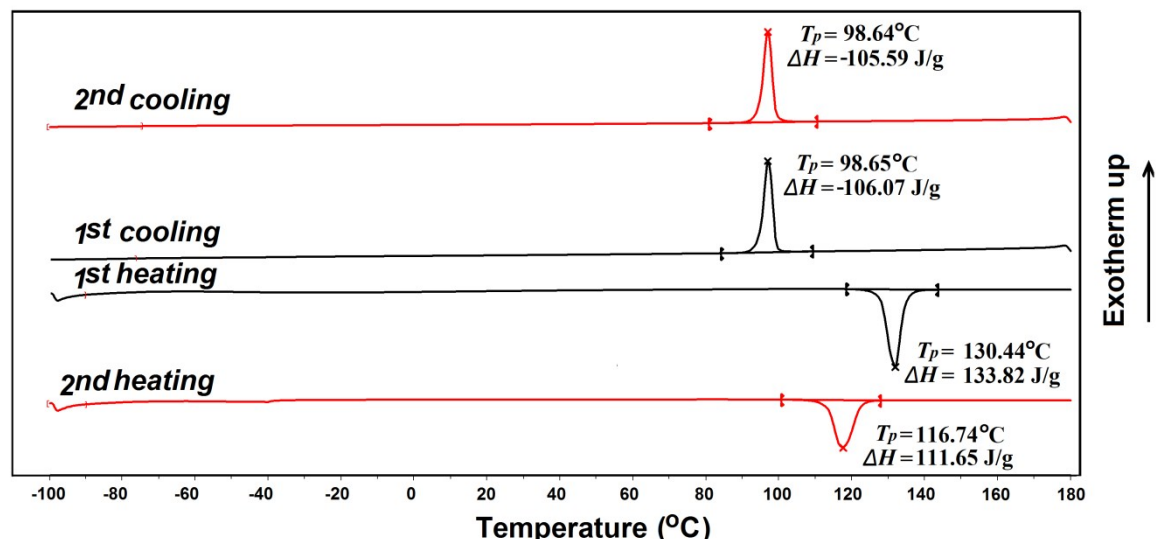


Figure S17. DSC curves of β -form, recorded with a heating and cooling rate of $20^\circ\text{C min}^{-1}$. Peak temperatures (T_p) and the heat of fusion (ΔH) are given in $^\circ\text{C}$ and J g^{-1} , respectively.

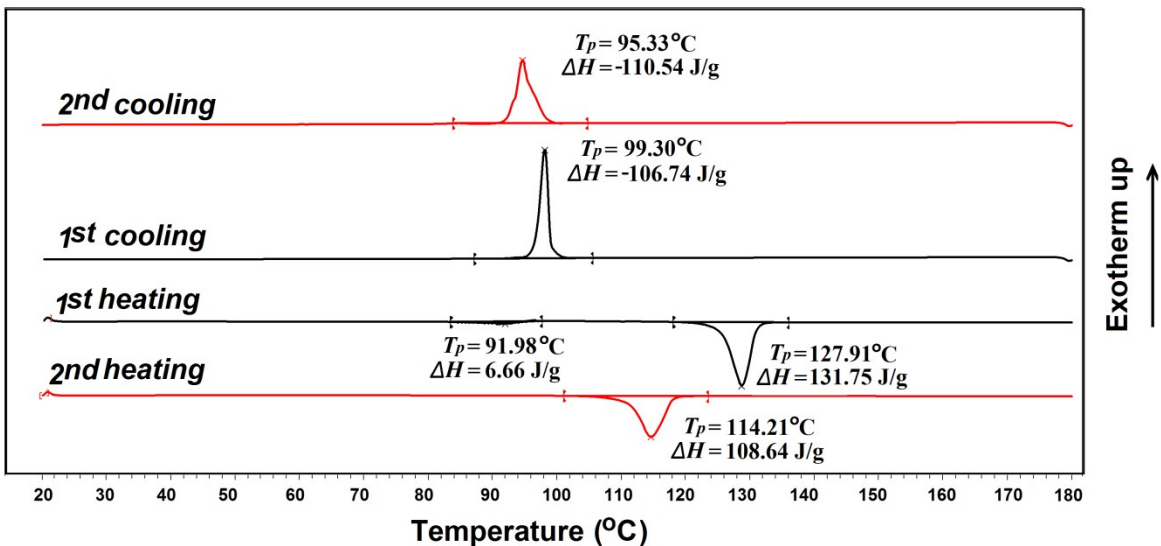


Figure S18. DSC curves of β -form, recorded with a heating and cooling rate of $10\text{ }^\circ\text{C min}^{-1}$. Peak temperatures (T_p) and the heat of fusion (ΔH) are given in ${}^\circ\text{C}$ and J g^{-1} , respectively.

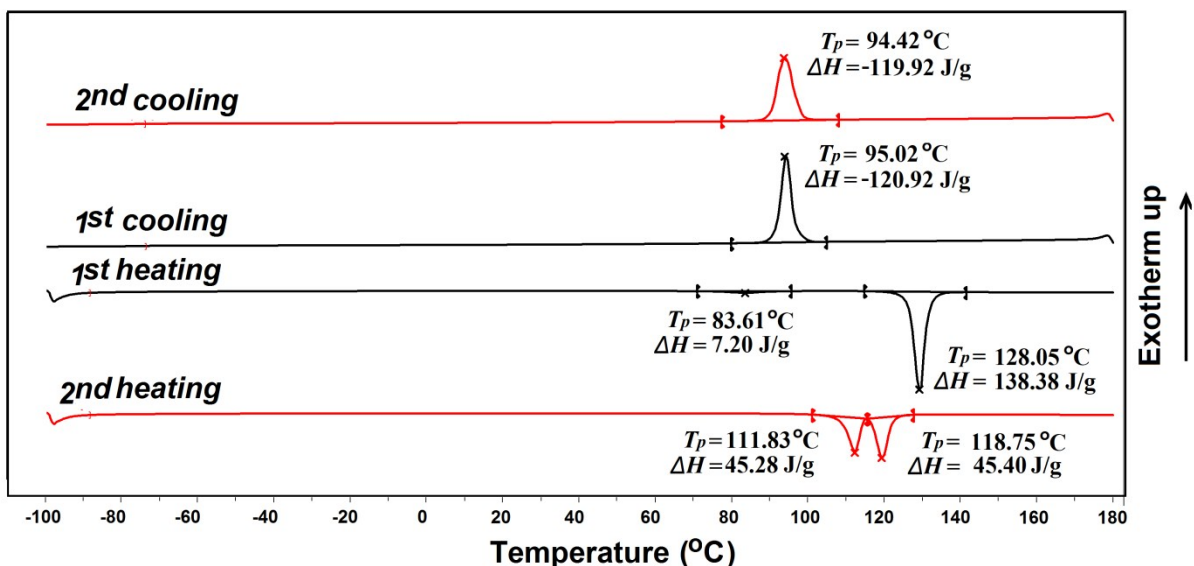


Figure S19. DSC curves of γ -form, recorded with a heating and cooling rate of $20\text{ }^\circ\text{C min}^{-1}$. Peak temperatures (T_p) and the heat of fusion (ΔH) are given in ${}^\circ\text{C}$ and J g^{-1} , respectively.

During the first heating with a heating rate of $20\text{ }^\circ\text{C min}^{-1}$, α - and β -forms exhibit solely melting at $129.42\text{ }^\circ\text{C}$ ($\Delta H_F = 134.80\text{ J g}^{-1}$) and $130.44\text{ }^\circ\text{C}$ ($\Delta H_F = 133.82\text{ J g}^{-1}$), respectively. The γ -form shows a phase transformation to α -form on heating at $83.61\text{ }^\circ\text{C}$ ($\Delta H_F = 7.20\text{ J g}^{-1}$) and melts at $128.05\text{ }^\circ\text{C}$ ($\Delta H_F = 138.38\text{ J g}^{-1}$). During the first heating with a heating rate of $10\text{ }^\circ\text{C min}^{-1}$, β -form converts to α -form at $91.98\text{ }^\circ\text{C}$ ($\Delta H_F = 6.66\text{ J g}^{-1}$) before melting at $127.91\text{ }^\circ\text{C}$ ($\Delta H_F = 131.75\text{ J g}^{-1}$).